Toward the Synthesis of Wafer-Scale Single-Crystal Graphene on Copper Foils

Zheng Yan,[†] Jian Lin,[‡,§] Zhiwei Peng,[†] Zhengzong Sun,[†] Yu Zhu,[†] Lei Li,[†] Changsheng Xiang,[†] E. Loïc Samuel,[†] Carter Kittrell,[†,‡] and James M. Tour[†,‡,§,*]

[†]Department of Chemistry, [‡]Richard E. Smalley Institute for Nanoscale Science and Technology, and [§]Department of Mechanical Engineering and Materials Science, Rice University, 6100 Main Street, Houston, Texas 77005, United States

ABSTRACT In this research, we constructed a controlled chamber pressure CVD (CP-CVD) system to manipulate graphene's domain sizes and shapes. Using this system, we synthesized large (~4.5 mm^2) single-crystal hexagonal monolayer graphene domains on commercial polycrystalline Cu foils (99.8% purity), indicating its potential feasibility on a large scale at low cost. The as-synthesized graphene had a mobility of positive charge carriers of ~11 000 $cm^2 V^{-1} s^{-1}$ on a SiO_2/Si substrate at room temperature, suggesting its comparable quality to that of exfoliated graphene. The growth mechanism of Cu-based graphene was explored by studying the influence of varied growth parameters on graphene domain sizes. Cu pretreatments, electrochemical polishing, and high-pressure annealing are shown to be critical for suppressing graphene nucleation site density. A pressure of 108 Torr was the optimal chamber pressure for the synthesis of large single-crystal monolayer graphene. The synthesis of one graphene seed was achieved on centimeter-sized Cu foils by optimizing the flow rate ratio of H_2/CH_4. This work should provide clear guidelines for the large-scale synthesis of wafer-scale single-crystal graphene, which is essential for the optimized graphene device fabrication.

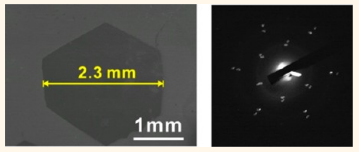

KEYWORDS: graphene · hexagonal · single-crystal · CP-CVD

Mechanically exfoliated graphene demonstrates extraordinary electrical and physical properties that could be harnessed to enable exceptional advances in technology.[1−3] However, the initially reported micromechanical exfoliation of highly oriented pyrolytic graphite can only yield a minute amount of small single-crystal graphene, limiting the practicality of this method.[1,2] Recently developed CVD methods could produce large-size and uniform polycrystalline graphene,[4−6] but the electronic properties of CVD graphene are degraded by domain boundaries.[7] Thus, the fabrication of large-size single-crystal graphene using CVD on transition metals, especially on Cu, has attracted much interest among materials scientists.[7−15] There have been advancements in the growth of Cu-based single-crystal graphene. For example, ~10 μm sized self-arrayed single-crystal graphene domains were fabricated by prepatterning seeds on Cu.[7,8] The ~100−200 μm sized hexagonal single-crystal graphene domains were made on melted Cu.[9,10] Submillimeter single-crystal graphene was successfully synthesized by preannealing Cu at atmospheric pressure[11] or using a Cu enclosure for graphene growth.[12] The ~100 μm sized single-crystal graphene flowers were also made by trapping vapor growth on Cu and controlling pressure.[13] Finally, the growth of millimeter-sized single-crystal graphene was recently achieved on Pt[14] and Ni.[15] However, the facile synthesis of graphene with larger single-crystal domains on commercial Cu is desirable. Recent research has been based on empirical optimization; however, the precise growth mechanism of the Cu-based graphene is not well-explored.[4−15]

RESULTS AND DISCUSSION

While the CVD chamber pressure is an important parameter for controlling graphene growth, most present research is focused on low-pressure and atmospheric-pressure CVD growth.[4−19] In this research, we constructed a CP-CVD system by adding a metering valve, as shown in Figure 1a, which can be used to precisely manipulate the chamber pressure, ranging from 1 mT to 1500 Torr. This modification allows us to adjust the chamber pressure during the annealing or growth process to control the shapes and sizes of graphene domains.

Using this system, the synthesis of large-size (~4.5 mm^2) single-crystal monolayer graphene on Cu was achieved as follows. Cu surfaces were first cleaned using the electrochemical polishing method (see Supporting Information) and then annealed at 1500 Torr and 1077 °C for 7 h with a H_2 flow rate of 500 sccm. After annealing, the flow rate of H_2 was decreased to 70 sccm and the chamber pressure was adjusted to ~108 Torr by the metering valve. The graphene

* Address correspondence to tour@rice.edu.

Received for review July 25, 2012 and accepted September 11, 2012.

Published online 10.1021/nn303352k

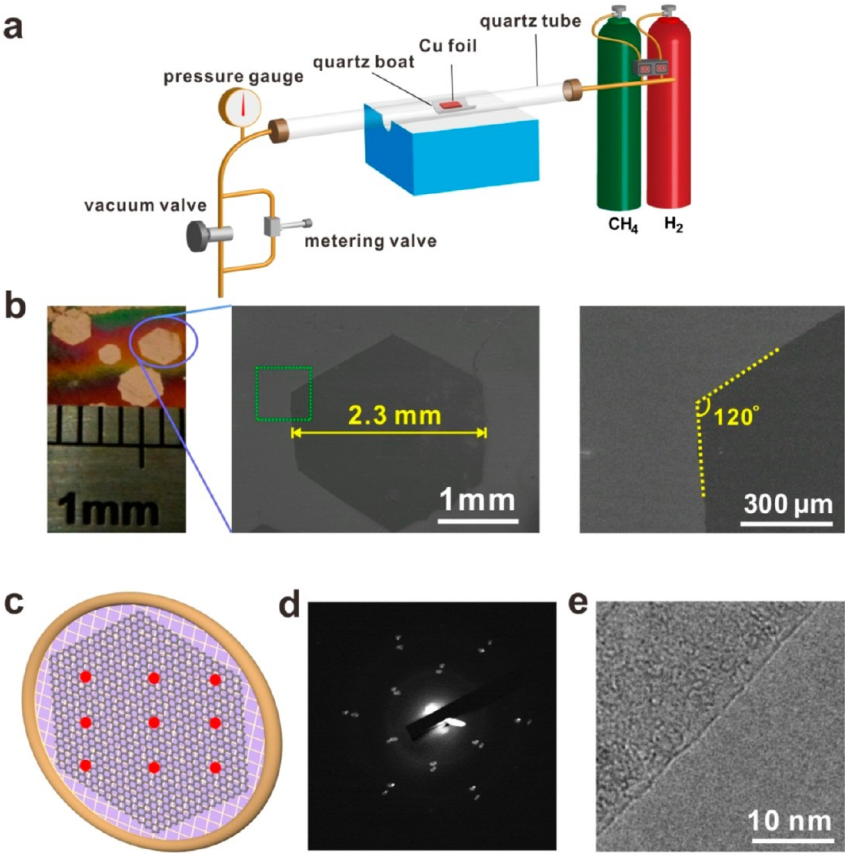

Figure 1. Synthesis of large-size (~2.3 mm) single-crystal graphene monolayer domains using the CP-CVD system. (a) Drawing of the CP-CVD system, where a metering valve was added to precisely manipulate the chamber pressure ranging from 1 mT to 1500 Torr. (b) Typical optical and SEM images of as-produced graphene domains on Cu. (c) SAED mapping protocol of the graphene transferred onto a TEM grid. The diameter of TEM grid was ~3 mm, and the distance between the nine adjacent selected points was ~0.5 mm. (d) Overlaid nine SAED patterns. The separate SAED patterns are shown in Figure S2 (Supporting Information). (e) HRTEM image randomly taken from the graphene domain edge, verifying that it is monolayered.

growth was started by introducing 0.15 sccm CH_4 into the chamber, with the H_2 held at 70 sccm, for 125 min. After the reaction, the Cu foils were quickly removed from the hot zone of the CVD furnace and permitted to cool to room temperature. This growth was performed on commercial polycrystalline Cu foils (99.8% purity, Alfa Aesar) without needing extremely low CH_4 concentrations,[7] a noble metal substrate such as Pt,[14] or ultrahigh vacuum,[15] indicating that this is a feasible and practical method for the scalable production of large-size single-crystal graphene at low cost.

After the graphene growth, the Cu foils were heated in air for 1 min at 215 °C; the oxidation of Cu foils makes the graphene domains optically visible.[11] Figure 1b is a typical optical image of a Cu surface after the graphene growth, showing four graphene domains in this ~7 mm × 7 mm area. Three of them are ~2.3 mm, and the middle domain is ~1 mm, suggesting that the graphene nucleus related to these four graphene domains did not form simultaneously. The SEM images in Figure 1b show that the obtained graphene domain is hexagonally shaped and has straight edges and well-identifiable 120° corners. Its edge-to-edge distance is ~2.3 mm, and the surface area is ~4.5 mm^2, more than 20 times larger than the best reported results on Cu.[11,12] Rough edges are sometimes observed in graphene domains (Figure S1) and arise from the mixture of zigzag and armchair terminations.[16,17]

In four different experiments, we halted the reactions after 10, 30, 60, or 125 min, as shown in Figure S1. In all of these cases, only one graphene domain was found in the ~3 mm × 3 mm region (Figure S1a–d). The growth rates were estimated from the SEM images and demonstrated in Figure S1e,f. The growth rate of edge-to-edge distance is relatively uniform, ~18 μm min^{-1}, under these experimental conditions (Figure S1e). However, Figure S1f indicates that the surface areas of graphene domains had an accelerated growth rate. This can be understood by the fact that, with the increase in the perimeters of the graphene domains, greater graphene edge lengths are exposed to the Cu foil, consequently leading to an increase in the amount of active carbon species captured by graphene edges per unit time.

Selected area electron diffraction (SAED) patterns have been widely used to characterize small-size single-crystal graphene domains.[7,11] However, a single

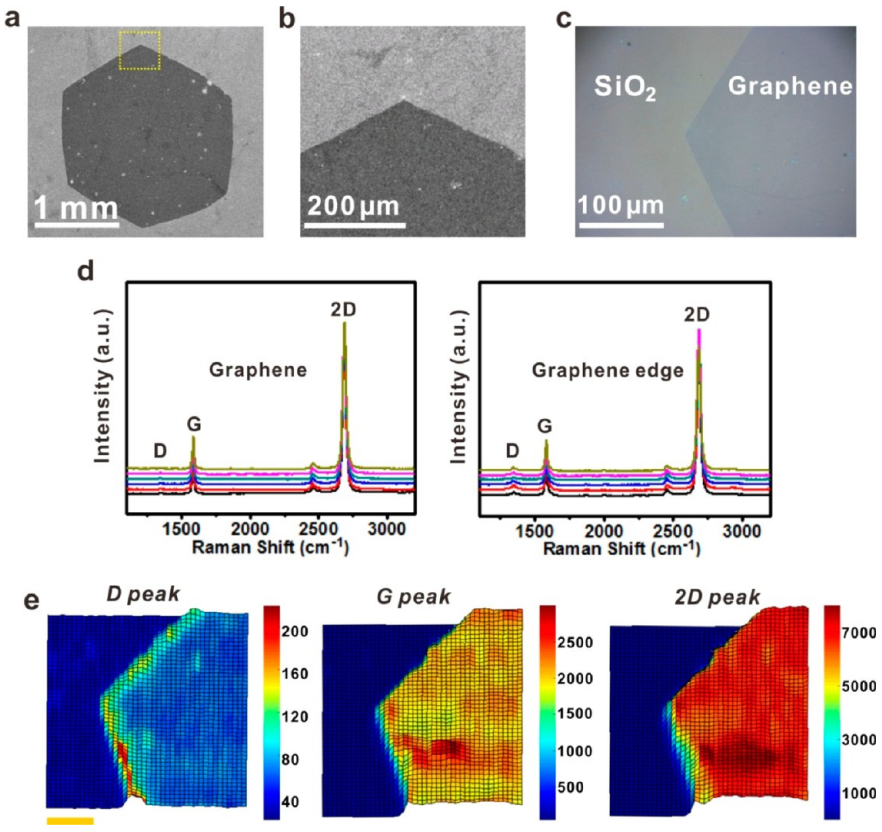

Figure 2. SEM and Raman spectroscopy characterizations of graphene domains transferred to SiO_2/Si wafers. (a) Typical SEM image of one graphene domain transferred onto SiO_2/Si. (b) Enlarged SEM image of the yellow squared region in (a). (c) Optical image taken from the corner of one graphene domain. (d) Raman spectra of graphene (left) and graphene edges (right), each showing spectra of six different spots. (e) Three-dimensional Raman maps of D peak, G peak, and 2D peak. The Raman mapping is performed on the graphene corner shown in (c), and the data are extracted from D (1350 cm^{-1}), G (1580 cm^{-1}), and 2D (2690 cm^{-1}) locations.[4−6] The scale bar is 5 μm.

SAED pattern analysis only covers a micrometer-sized area of graphene. In order to analyze these large-size graphene domains, a SAED mapping pattern was performed across the entire graphene and nine different points were selected, as shown in Figure 1c. The distance between adjacent points is ~0.5 mm. All of the SAED patterns of these nine points had the same orientations (Figure S2) and were overlaid to produce a combined pattern (Figure 1d), indicating a single-crystalline lattice structure. The slight offset in the SAED patterns is occasionally observed because of the intrinsic corrugation in the graphene flake or accidental folding introduced during the transfer.[7,11,12] The high-resolution TEM (HRTEM) image in Figure 1e was randomly taken from numerous graphene domain edges. The layer count on the edge of the HRTEM image indicates that as-grown graphene is monolayered.

As-produced graphene was transferred onto SiO_2/Si wafers for further characterization (see Supporting Information). Figure 2a is a typical SEM image of the graphene domain on the SiO_2/Si wafer. Figure 2b,c shows the SEM and optical images taken from corners of different graphene samples. The clean surfaces shown in Figure 2a−c demonstrate that residual PMMA has been removed following the transfer process. All of these SEM and optical images demonstrate uniform color contrast, suggesting that uniform monolayer graphene was obtained. The straight edges and 120° corners indicate that the original shapes of the transferred graphene samples are preserved.

Raman spectroscopy was done on the transferred graphene samples to evaluate their quality and thickness. Figure 2d shows the Raman spectra recorded at 12 different spots from the graphene in Figure 2a, six within the graphene and six over the graphene edge. The Raman spectra indicate that the D peaks within the graphene are in the noise level, signifying the presence of few defects and that it has high quality, comparable to that of the exfoliated graphene.[20] The D peaks recorded from the graphene edges are slightly higher than those within the graphene and are thought to arise from the lower symmetry of the edges.[16,17] In all of these 12 Raman spectra, the intensities of 2D peaks are more than twice those of G peaks and the full widths at half-maximum (fwhm) of the 2D peaks are ~30 cm^{-1}, suggesting that the as-produced samples are monolayer graphene.[4,20]

Raman mapping provides a direct, statistically sound method to confirm the quality, thickness, and uniformity of graphene samples.[6] Therefore, Raman mapping was performed on the graphene corner shown in

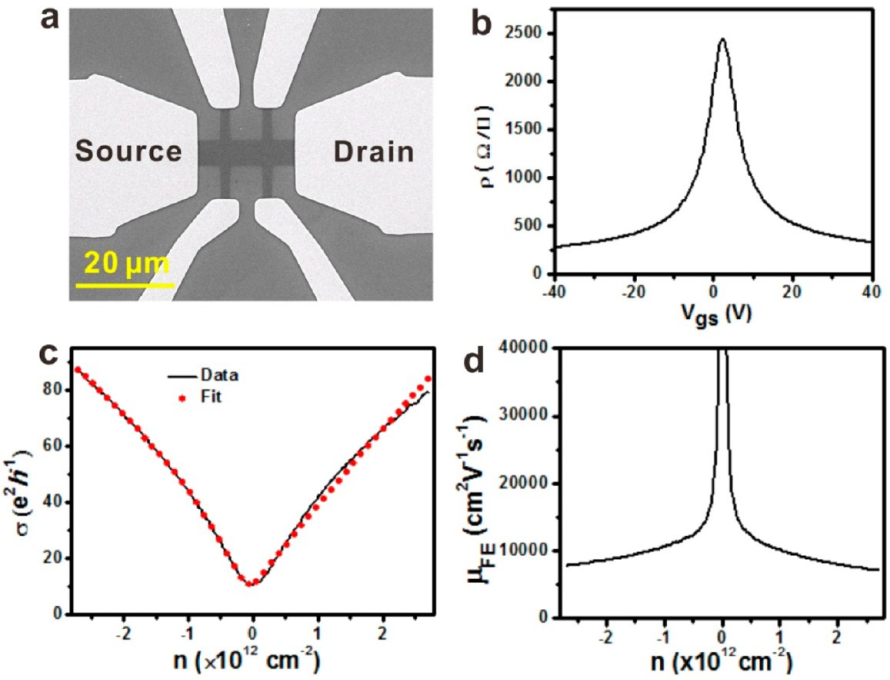

Figure 3. Graphene Hall bar device with resistivity, conductivity, and mobility from a FET measured at 300 K. (a) SEM image of a graphene Hall bar FET on a SiO_2/Si substrate. (b) Resistivity of graphene *versus* the back gate voltage. (c) Conductivity of graphene as a function of carrier density. The collected data are plotted as a black line, while the data fitted by a Boltzmann model are indicated by the red filled circles. (d) Plot of the density-dependent field effect mobility of graphene as a function of carrier density.

Figure 2c; the step size was 0.5 μm, and the investigated region was ~25 μm × 25 μm. Three-dimensional Raman maps of D (1350 cm^{-1}), G (1580 cm^{-1}), and 2D (2690 cm^{-1}) peaks were extracted and plotted in Figure 2e, where different colors indicate different intensities (I_x, where x = D, G, or 2D). Figure 2e shows that I_D is negligibly small over the area of the graphene, with the exception of the edges, revealing that the as-grown graphene sample was almost defect-free.[20] The graphene edges have relatively large D peaks in the spectra, and the ratio of the I_D to I_G peak is ~0.1, consistent with previous studies of graphene edges, suggesting that the edges are dominated by zigzag terminations.[16,17] Figure 2e shows that I_G and I_{2D} are relatively uniform and that I_{2D} is more than twice as large as I_G over the graphene corner, indicating complete monolayer graphene coverage in the investigated region.[4,20] Interestingly, small second- and third-layer graphene regions were occasionally observed on the large monolayer graphene domains, indicating a terraced structure (Figure S3). We attribute the formation of this special structure to the self-limiting mechanism of graphene growth, meaning that after the coverage of carbon on the Cu surface, the next-layer graphene growth is extremely limited.[4]

To evaluate the quality of single-crystal graphene domains, Hall bar FETs with a highly doped p-type silicon back gate were fabricated (see Supporting Information). Figure 3a shows the SEM image of a fabricated Hall bar FET device. The plot of resistivity *versus* back gate voltage, V_{gs}, is shown in Figure 3b, indicating that the ON/OFF ratio is ~10. The device exhibits low resistivity (270 Ω/□) at high carrier density and a sharp resistivity peak of 2.5 kΩ/□ at the Dirac point (V_{Dirac} = 2.4 V). The conductivity σ *versus* carrier density n (given by $n = C_g(V_{gs} - V_{Dirac})/e$, C_g = 11.5 nF/cm^2) is shown in Figure 3c, which exhibits almost linear σ for both positive and negative carriers. To further characterize the transport characteristic of the single-crystal graphene device, a commonly used self-consistent Boltzmann theory[21,22] was used that includes long- and short-range scattering sources to fit the conductivity: $\sigma^{-1} = (\mu_c ne + \sigma_0)^{-1} + \rho_s$. In this model, μ_c denotes the density-independent charge mobility corresponding to the long-range scattering; ρ_s is the resistivity contributed from short-range scattering; and σ_0 is the residual conductivity at the Dirac point. From the data, fitted as shown in Figure 3c, the density-independent charge mobility can be extracted to give μ_c = 10 400 $cm^2 V^{-1} s^{-1}$ for positive charge carriers. The extracted density-independent mobilities for positive charge carriers, from a total of 10 tested devices, ranged from 7900 to 11000 $cm^2 V^{-1} s^{-1}$. These high mobilities within a relatively narrow range indicate an electrical performance comparable to that of exfoliated graphene on a SiO_2 substrate. Figure 3d is the density-dependent field effect mobility $\mu_{FE} = \sigma/ne$, using a simple Drude model.[1,2] For positive charge carriers, μ_{FE} spans from 8600 $cm^2 V^{-1} s^{-1}$ at a carrier density of 2 × 10^{12} cm^{-2} to greater than 12 500 $cm^2 V^{-1} s^{-1}$ at a density less

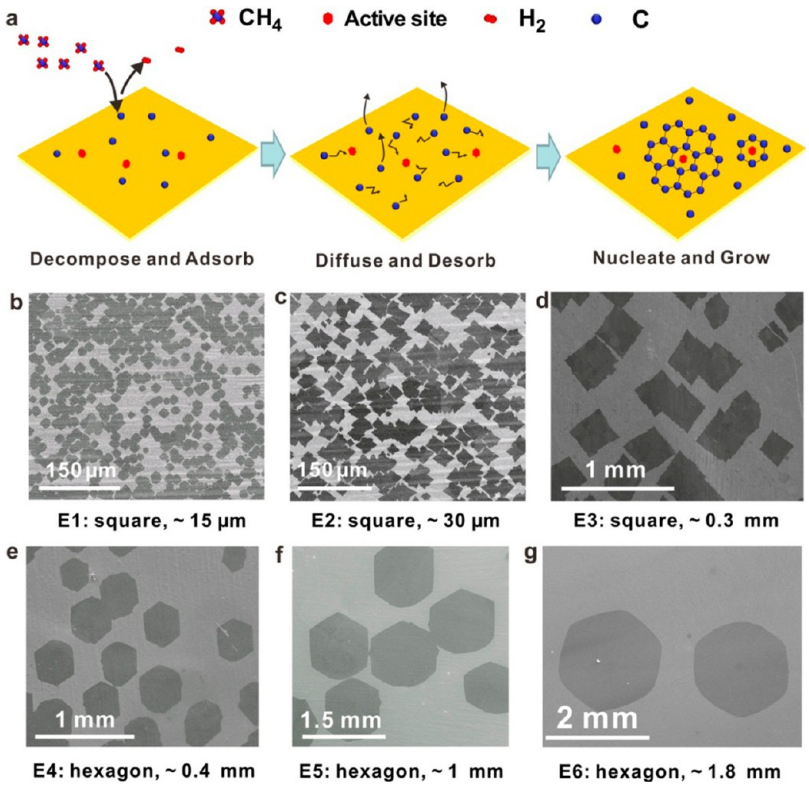

Figure 4. Illustration of the Cu-based graphene growth mechanism and the influence of different parameters on the graphene domain sizes and shapes. (a) Scheme for the Cu-based graphene growth mechanism. Here, red hexagons are used to symbolize the active sites of the Cu surface, and blue spots signify active carbon species $(CH_{x<4})_s$. From the proposed mechanism, the active carbon species from the dissociated CH_4 are apt to agglomerate into thermodynamically stable $(C_nH_y)_s$ species on the active sites of the Cu surface to initialize the graphene growth. (b–g) Typical SEM images of graphene synthesized under different growth conditions: b (E1), c (E2), d (E3), e (E4), f (E5), and g (E6).

than 5×10^{11} cm^{-2}. Overall, the high electrical performance of the graphene devices indicates the high quality of the as-grown single-crystal graphene. The carrier mobility is larger than those of recently reported single-crystal graphene on Si/SiO_2 substrates.[7,10,12−14] The carrier mobility of the as-produced graphene can likely be further improved by using boron nitride substrates[22] or by fabricating suspended devices.[23,24]

The growth of graphene is restricted to the catalyst surface due to the low solubility of carbon in Cu (<0.001 atom %);[19] the process demonstrated here might be feasible for the production of wafer-sized single-crystal graphene. To reach this goal, the most challenging tasks are the development of a deep understanding of the mechanism of graphene growth and the probable requirement for a single seed of graphene to start the growth. On the basis of the data presented here, we propose a growth mechanism for Cu-based graphene (Figure 4a) and demonstrate reaction conditions that reduce the graphene nucleation density and allow the growth of larger-size graphene domains using an extended growth period (Figure 4b–g and Table S1 and Figure S4 in the Supporting Information).

The overall growth processes for Cu-based graphene are described in Figure 4a; to illustrate the process, it is divided into three main steps. Red hexagons are used to symbolize the active sites of the Cu surface, such as impurities, sharp wrinkles, and defects, which are known to act as active heteronuclei in the early stages of graphene growth.[7,11,25] (1) CH_4 dissociates and is chemically adsorbed on the Cu surface to form the active carbon species $(CH_{x<4})_s$,[26,27] where "s" signifies "surface-adsorbed" to distinguish it from a gaseous molecule. The exact nature of the active carbon species has not been well-defined,[17,18] and we used carbon monomers (C) to represent all types of active carbon species in Figure 4a. (2) From recent research, the carbon–Cu interaction is weak and the desorption rate of active carbon species is comparable to its mobility on the Cu surface above 870 °C.[18] Under the growth conditions described in this paper, the temperature is >1000 °C, suggesting that the movement of active carbon species on the Cu surface is dominated by diffusion and desorption. (3) Theoretical calculations show that active carbon species are thermodynamically unstable and tend to agglomerate into thermodynamically stable $(C_nH_y)_s$ species on the active sites of the Cu surface,[27] ultimately leading to the formation of graphene nuclei. Once the graphene nuclei are formed, most of the active carbon species will be captured and consumed in the growth of graphene, reducing the probability

that new graphene nuclei will be formed in the nearby areas of the Cu catalyst.

From the data that have been presented, reducing the concentrations of both active sites and active carbon species on the Cu surface is the key factor in reducing graphene nuclei density, enabling the growth of larger-size graphene domains during the extended growth time. On the basis of this mechanism, we explored the influences of several parameters on the graphene domain sizes. Eleven growth experiments (E1−E11) were performed; they are listed in Table S1 in Supporting Information. For every experiment, the same temperatures were used in the annealing and growth processes. The relationship between graphene domain sizes and growth conditions is plotted in Figure S4.

In the following experiments, we stopped the graphene growth before a continuous film formed in order to directly demonstrate the shapes and sizes of as-grown graphene domains under different growth conditions.[7−14] We began the experimental series with E1, which is the CVD-based graphene growth condition that was generally used in our laboratory. Under the conditions of E1, the obtained graphene domains were square and the domain sizes were ∼15 μm (Figure 4b and Figure S5). In E2, the CH_4 flow rate was lowered to 0.15 sccm, and the flow rate ratio of H_2 to CH_4 was increased to ∼460; both contributed to diluting the concentration of active carbon species on the Cu surface. In this case, the graphene domain sizes increase to ∼30 μm after extended periods of time (Figure 4c). From E3 to E10, electrochemical polishing and high-pressure annealing were used to improve the quality of the Cu. Electrochemical polishing[25,28] cleans the Cu surface and removes the impurity layer (Figure S6); high-pressure annealing can eliminate sharp wrinkles, steps, and defects to improve the quality of the Cu (Figure S7). Both apparently reduced the Cu surface active sites and consequently decreased the graphene nucleus density. Figure 4d shows that the graphene domain size increased to ∼0.3 mm on the electrochemically polished and high-pressure annealed Cu substrates (E3) when other conditions are similar to those of E2. In this case, the graphene domain shapes are still square.

The graphene domain shapes become hexagonal when adjusting the chamber pressure to ∼108 Torr during the growth process (E4−E11 and Figure 4e−g). The shape evolution is attributed to the fact that H_2 has different etching abilities on zigzag and armchair terminations at different H_2 partial pressures and temperatures.[7,17,29] A detailed study of the dependence of the shapes and thickness of graphene domains on various chamber pressures and temperatures is a subject of our future investigations.

Interestingly, the graphene domain sizes further increased when raising annealing and growth temperatures (E5−E7, Figure 1b, Figure S1, and Figure 4e−g). Figure 4e−g shows that the sizes of the graphene domains increased from ∼0.4 to ∼1 and ∼1.8 mm as the temperature increased from 1060 °C (E4, Figure 4e) to 1070 °C (E5, Figure 4f) and 1075 °C (E6, Figure 4g). The higher growth temperature reduces the concentration of active carbon species on the Cu surface by speeding desorption,[18] and the higher annealing temperature improves the quality of Cu substrates.[30] Both of these contributed to the reduction of the graphene nucleation density and consequently the increase of the graphene domain sizes in the extended growth time. A temperature of 1077 °C (E7, Figure 1b and Figure S1) is the limit of our CP-CVD system, and in this case, the graphene domain sizes increased to ∼2.3 mm. Moreover, graphene synthesized using the conditions of E7 has a cleaner and flatter surface than those of graphene obtained using E1 (Figure S8), suggesting its improved quality.

Interestingly, when the flow rate of H_2 was increased to 150 sccm from 70 sccm to dilute CH_4 (E8), only one graphene nucleus was found on ∼1 cm × 1 cm Cu after 90 min growth (Figure S9). Moreover, no graphene nucleus was found on ∼1 cm × 1 cm Cu after 125 min growth when further increasing the flow rate of H_2 to 200 sccm (E9). Limited by our simple 1 in. quartz tube furnace, additional optimizations were not performed. Meanwhile, the slow edge-to-edge growth speed of the graphene domain (∼1 μm min^{-1}) under E8 also placed an obstacle for the final synthesis of centimeter-size single-crystal graphene. Moreover, if this process could be conducted in a cleanroom to minimize exogenous carbon impurities on the foil, then even larger domains would be expected. However, these two experiments (E8 and E9) indicate the possibility of one-seed requirement on the wafer-scale Cu through further optimizations of growth conditions. In addition, the control experiments (E10 and E11) in Figure S10 demonstrate that the combination of Cu surface electrochemical polishing and high-pressure annealing are necessary for the synthesis of high-quality and large-size single-crystal graphene. Figure S11 demonstrates that graphene domains can grow across Cu grain boundaries, suggesting the weak influence of Cu grain size on graphene growth.[7]

CONCLUSION

In conclusion, we have reported the practical and feasible synthesis of large-size (∼4.5 mm^2) single-crystal monolayer graphene using a CP-CVD method on commercial Cu foils. The as-produced graphene samples are clean, flat, and hexagonal-shaped. TEM, SEM, and Raman spectroscopy were used to characterize the obtained graphene, suggesting that their high quality is comparable to that of exfoliated graphene. Hall bar FETs were fabricated using the as-grown graphene, showing a mobility of positive charge carriers of ∼11 000 cm^2 V^{-1} s^{-1} on a SiO_2/Si substrate at

room temperature. In addition, the Cu graphene growth mechanism was explored, and optimization resulted in the increase of the graphene domain from ~15 μm to ~2.3 mm, reaching ~10% of a 1 in. silicon wafer size. Moreover, in the optimized growth conditions, one graphene seed requirement was achieved on the centimeter-size Cu foils. Additional optimization was not done because of limitations in our CVD system, which is restricted to a simple 1 in. quartz tube furnace. However, the controlled studies here will underpin improvements that can lead to the viable synthesis of wafer-scale single-crystal graphene.

METHODS

SAED and HRTEM were done using a JEOL 2100-F operated at 200 keV. SEM was done using a JEOL6500 scanning electron microscope at 15 keV. The Raman spectra were recorded with a Renishaw Raman RE01 scope using a 514 nm excitation argon laser. A six-probe station (model FWPX, Desert Cryogenics-LakeShore) was used to measure the electrical properties under vacuum (10^{-5}–10^{-6} Torr). An Agilent 4155C semiconductor parameter analyzer was used to record the I–V data.

Conflict of Interest: The authors declare no competing financial interest.

Acknowledgment. The authors thank J. Yao, C. Zhang, and A. O. Raji for discussions, and G. Bond for his help in electrochemical polishing Cu. This project was funded by the ONR MURI program (#00006766, N00014-09-1-1066); the Lockheed Martin Corporation through the LANCER IV Program; the Air Force Office of Scientific Research (FA9550-09-1-0581); and the AFOSR MURI (FA9550-12-1-0035).

Supporting Information Available: Further details are provided related to graphene growth procedures, graphene transfer method, electrochemical polishing method, and device fabrication. This material is available free of charge *via* the Internet at http://pubs.acs.org.

REFERENCES AND NOTES

1. Zhang, Y. B.; Tan, Y. W.; Stormer, H. L.; Kim, P. Experimental Observation of the Quantum Hall Effect and Berry's Phase in Graphene. *Nature* **2005**, *6*, 201–204.
2. Novoselov, K. S.; Geim, A. K.; Morozov, S. V.; Jiang, D.; Zhang, Y.; Dubonos, S. V.; Grigorieva, I. V.; Firsov, A. S. Electric Field Effect in Atomically Thin Carbon Films. *Science* **2004**, *306*, 666–669.
3. Geim, A. K.; Novoselov, K. S. The Rise of Graphene. *Nat. Mater.* **2007**, *6*, 183–191.
4. Li, X. S.; Cai, W.; An, J.; Kim, S.; Nah, J.; Yang, D.; Piner, R.; Velamakanni, A.; Jung, I.; Tutuc, E.; *et al.* Large-Area Synthesis of High-Quality and Uniform Graphene Films on Copper Foils. *Science* **2009**, *324*, 1312–1314.
5. Bae, S.; Kim, H.; Lee, Y.; Xu, X.; Park, J.; Zheng, Y.; Balakrishnan, J.; Lei, T.; Kim, H. R.; Song, Y.; *et al.* Roll-to-Roll Production of 30-Inch Graphene Films for Transparent Electrodes. *Nat. Nanotechnol.* **2010**, *5*, 574–578.
6. Sun, Z.; Yan, Z.; Jun, Y.; Beitler, E.; Zhu, Y.; Tour, J. M. Growth of Graphene from Solid Carbon Sources. *Nature* **2010**, *468*, 549–552.
7. Yu, Q.; Jauregui, L. A.; Wu, W.; Colby, R.; Tian, J.; Su, Z.; Cao, H.; Liu, Z.; Pandey, D.; Wei, D.; *et al.* Control and Characterization of Individual Grains and Grain Boundaries in Graphene Grown by Chemical Vapor Deposition. *Nat. Mater.* **2011**, *10*, 443–449.
8. Wu, W.; Jauregui, L. A.; Su, Z.; Liu, Z.; Bao, J.; Chen, Y. P.; Yu, Q. Growth of Single Crystal Graphene Arrays by Locally Controlling Nucleation on Polycrystalline Cu Using Chemical Vapor Deposition. *Adv. Mater.* **2011**, *23*, 4898–4903.
9. Wu, Y. A.; Fan, Y.; Speller, S.; Greeth, G. L.; Sadowski, J. T.; He, K.; Robertson, A. W.; Allen, C. S.; Warner, J. H. Large Single Crystals of Graphene on Melted Copper Using Chemical Vapor Deposition. *ACS Nano* **2012**, *6*, 5010–5017.
10. Geng, D.; Wu, B.; Guo, Y.; Huang, L.; Xue, Y.; Chen, J.; Yu, G.; Jiang, L.; Hu, W.; Liu, Y. Uniform Hexagonal Graphene Flakes and Films Grown on Liquid Copper Surface. *Proc. Natl. Acad. Sci. U.S.A.* **2012**, *109*, 7992–7996.
11. Wang, H.; Wang, G.; Bao, P.; Yang, S.; Xie, X.; Zhang, W. Controllable Synthesis of Submillimeter Single-Crystal Monolayer Graphene Domains on Copper Foils by Suppressing Nucleation. *J. Am. Chem. Soc.* **2012**, *134*, 3627–3630.
12. Li, X.; Magnuson, C. W.; Venugopal, A.; Tromp, R. M.; Hannon, J. B.; Vogel, E. M.; Colombo, L.; Ruoff, R. S. Large-Area Graphene Single Crystals Grown by Low-Pressure Chemical Vapor Deposition of Methane on Copper. *J. Am. Chem. Soc.* **2011**, *133*, 2816–2819.
13. Zhang, Y.; Zhang, L.; Kim, P.; Ge, M.; Li, Z.; Zhou, C. Vapor Trapping Growth of Single-Crystalline Graphene Flowers: Synthesis, Morphology, and Electronic Properties. *Nano Lett.* **2012**, *12*, 2810–2816.
14. Gao, L.; Ren, W.; Xu, H.; Lin, L.; Wang, Z.; Ma, T.; Ma, L.; Zhang, Z.; Fu, Q.; Peng, L.; *et al.* Repeated Growth and Bubbling Transfer of Graphene with Millimeter-Size Single-Crystal Grains Using Platinum. *Nat. Commun.* **2012**, DOI: 10.1038/ncomms1702.
15. Iwasaki, T.; Park, H. J.; Konuma, M.; Lee, D. S.; Smet, J. H.; Starke, U. Long-Range Ordered Single-Crystal Graphene on High-Quality Heteroepitaxial Ni Thin Films Grown on MgO(111). *Nano Lett.* **2011**, *11*, 79–84.
16. Luo, Z.; Kim, S.; Kawamoto, N.; Rappe, A. M.; Johnson, A. T. C. Growth Mechanism of Hexagonal-Shape Graphene Flakes with Zigzag Edges. *ACS Nano* **2011**, *5*, 9154–9160.
17. Vlassiouk, I.; Regmi, M.; Fulvio, P.; Dai, S.; Datskos, P.; Eres, G.; Smirnov, S. Role of Hydrogen in Chemical Vapor Deposition Growth of Large Single-Crystal Graphene. *ACS Nano* **2011**, *5*, 6069–6076.
18. Kim, H.; Mattevi, C.; Calvo, M. R.; Oberg, J. C.; Artiglia, L.; Agnoli, S.; Hirjibenhedin, C. F.; Chhowalla, M.; Saiz, E. Activation Energy Paths for Graphene Nucleation and Growth on Cu. *ACS Nano* **2012**, *6*, 3614–3623.
19. Bhaviripudi, S.; Jia, X.; Dresselhaus, M. S.; Kong, J. Role of Kinetic Factors in Chemical Vapor Deposition Synthesis of Uniform Large Area Graphene Using Copper Catalyst. *Nano Lett.* **2010**, *10*, 4128–4133.
20. Ferrari, A. C.; Meyer, J. C.; Scardaci, V.; Casiraghi, C.; Lazzeri, M.; Mauri, F.; Piscanec, S.; Jiang, D.; Novoselov, K. S.; Roth, S. Raman Spectrum of Graphene and Graphene Layers. *Phys. Rev. Lett.* **2006**, *97*, 187401–187404.
21. Hwang, E. H.; Adam, S.; Sarma, S. D. Carrier Transport in Two Dimensional Graphene Layers. *Phys. Rev. Lett.* **2007**, *18*, 98.
22. Dean, C. R.; Young, A. F.; Meric, I.; Lee, C.; Wang, L.; Sorgenfrie, S.; Watanabe, K.; Taniguchi, T.; Kim, P.; Shepard, K. L.; *et al.* Boron Nitride Substrates for High-Quality Graphene Electronics. *Nat. Nanotechnol.* **2010**, *5*, 722–726.
23. Du, X.; Skachko, I.; Barker, A.; Andrei, E. Y. Approaching Ballistic Transport in Suspended Graphene. *Nat. Nanotechnol.* **2008**, *3*, 491–495.
24. Bolotin, K. I.; Sikes, K. J.; Jiang, Z.; Klima, M.; Fudenberg, G.; Hone, J.; Kim, P.; Stormer, H. L. Ultrahigh Electron Mobility in Suspended Graphene. *Solid State Commun.* **2008**, *146*, 351–355.
25. Luo, Z.; Lu, Y.; Singer, D. W.; Berck, M. E.; Somers, L. A.; Goldsmith, B. R.; Johnson, A. T. C. Effect of Substrate Roughness and Feedstock Concentration on Growth of Wafer-Scale Graphene at Atmospheric Pressure. *Chem. Mater.* **2011**, *23*, 1441–1447.

26. Wesep, R. V.; Chen, H.; Zhu, W.; Zhang, Z. Communication: Stable Carbon Nanoarches in the Initial Stages of Epitaxial Growth of Graphene on Cu(111). *J. Chem. Phys.* **2011**, *134*, 171105.
27. Zhang, W.; Wu, P.; Li, Z.; Yang, J. First-Principles Thermodynamics of Graphene Growth on Cu Surfaces. *J. Phys. Chem. C* **2011**, *115*, 17782–17787.
28. Zhang, B.; Lee, W. H.; Piner, R.; Kholmanov, I.; Wu, Y.; Li, H.; Ji, H.; Ruoff, R. S. Low-Temperature Chemical Vapor Deposition Growth of Graphene from Toluene on Electropolished Copper Foils. *ACS Nano* **2012**, *6*, 2471–2476.
29. Zhang, Y.; Li, Z.; Kim, P.; Zhang, L.; Zhou, C. Anisotropic Hydrogen Etching of Chemical Vapor Deposited Graphene. *ACS Nano* **2012**, *6*, 126–132.
30. Ajmal, M.; Lee, S.; Cho, Y. C.; Kim, S. J.; Park, S. E.; Cho, C. R.; Jeong, S. Fabrication of the Best Conductor from Single-Crystal Copper and the Contribution of Grain Boundaries to the Debye Temperature. *CrystEngComm* **2012**, *14*, 1463–1467.